ISSN 0036-0236, Russian Journal of Inorganic Chemistry, 2023, Vol. 68, No. 3, pp. 239–246. © Pleiades Publishing, Ltd., 2023.
ISSN 0036-0236, Russian Journal of Inorganic Chemistry, 2023. © Pleiades Publishing, Ltd., 2023.
Russian Text © The Author(s), 2023, published in Zhurnal Neorganicheskoi Khimii, 2023, Vol. 68, No. 3, pp. 291–299.

SYNTHESIS AND PROPERTIES OF INORGANIC COMPOUNDS

Synthesis and Investigation of $Na_{1-x}R_{0.33x}TiO_2(PO_4)_3$ (R = Y or La) Phosphates

V. A. Sedov[a], *, Ya. B. Glyadelova[a], E. A. Asabina[a], and V. I. Pet'kov[a]

[a] *Nizhny Novgorod State University, Nizhny Novgorod, 603022 Russia*

**e-mail: airbox200@gmail.com*

Received August 30, 2022; revised October 3, 2022; accepted October 14, 2022

Abstract—Phosphates $Na_{1-x}R_{0.33x}Ti_2(PO_4)_3$ (R = Y or La; $0 \le x \le 1$) were synthesized by the Pechini process and characterized by X-ray diffraction, electron microscopy with microprobe analysis, and IR spectroscopy. The systems exhibit isodimorphism to form a series of solid solutions belonging to the $NaZr_2(PO_4)_3$ (NZP) structural type and crystallizing in space group $R\bar{3}c$ or $R\bar{3}$. The Rietveld structural studies confirmed the isomorphic miscibility of sodium and the rare-earth element in the interstices of the NZP structure. The unit cell parameter c in the phosphates studied tends to increase, and the parameter a tends to decrease, in response to rising temperature, which trends are typical of NZP phosphates.

Keywords: NZP, phase formation, structure, thermal expansion, rare-earth elements

DOI: 10.1134/S0036023622602434

INTRODUCTION

Interest in phosphates of the $NaZr_2(PO_4)_3$ (NZP/NASICON) structural type is due to their potential for use as high-tech ceramic materials with tunable thermal expansion, including low values; they can be used in items requiring high thermal shock resistance [1–4] and in solid materials with high ionic conductivity [5], which are in demand for the design of rechargeable batteries [6]. In addition, NZP phosphates containing rare-earth elements (REE) are used as converters of UV rays, X-rays, and gamma-rays to the visible light [7–9]; as biologically compatible additives for the detection and imaging of tumors [10]; and as luminescent materials [11–16] resistant to damaging environmental factors.

The crystal structures of $NaZr_2(PO_4)_3$ [17] and $NaTi_2(PO_4)_3$ [18] are three-dimensional frameworks built of ZrO_6 (TiO_6) octahedra and PO_4 tetrahedra, which form columns lying parallel to one another. The cavities inside the columns are populated by Na^+ ions. The incorporation of cations(3+) into interstices of the NZP structure distorts the unit cell symmetry compared to the parent structure [19–23]. In $R_{0.33}Zr_2(PO_4)_3$ (R = Y, La, ... Lu) samples, for examples, cationic positions located in the cavities inside the columns of polyhedra are split into three types, and R^{3+} cations orderly populate one of them. The cell symmetry in REE-containing phosphates lowers from space group $R\bar{3}c$ of the parent structure to $P\bar{3}$ (for La [20]) or $P\bar{3}c$ (for Ce–Lu and Y [19]). Limited solid solutions $A_{1-x}Eu_{0.33x}Zr_2(PO_4)_3$ (A = Na, K, or Rb), which have different unit cell symmetries, were observed for both end-members [24].

The studies of $R_{0.33}Ti_2(PO_4)_3$ (R = La, Pr, or Gd) phosphates [25, 26] showed that the interstitial positions inside polyhedral columns are split into two types, where one type is 2/3 populated by REE ions and the other remain vacant. The alternation of these two types of interstices is implemented within the framework of the NZP structure with space group $R\bar{3}$.

Obviously, the reason for the difference between the structures of zirconium and titanium phosphates containing rare-earth elements lies in the sizes of the framework-forming ZrO_6 or TiO_6 octahedra (the ionic radius is 0.72 Å for Zr^{4+} and 0.61 Å for Ti^{4+} [27]). In this regard, it was of interest to study the effect of the framework-forming cations on phase formation and the properties of triple phosphates of alkali and rare-earth elements. The purpose of this work was to study the phase formation, structure, and thermal expansion of $Na_{1-x}R_{0.33x}Ti_2(PO_4)_3$ phosphates. Since the REE ionic radii in octahedrally coordinated interstices vary in the range of 0.87–1.03 Å, yttrium (0.90 Å) and lanthanum (1.03 Å) were chosen as the R elements substituting for sodium.

EXPERIMENTAL

The $Na_{1-x}R_{0.33x}Ti_2(PO_4)_3$ (R = Y or La; $0 \le x \le 1$) samples were synthesized by the Pechini method [28]. The chemicals used were at least of chemically pure grade (Table 1): Y_2O_3, $LaCl_3 \cdot 7H_2O$, $TiOCl_2$, $NH_4H_2PO_4$,

Table 1. Characteristics of the chemicals used for the synthesis

Chemical	Manufacturer	Weight fraction, %
Y_2O_3	KENO trading	>99.999
$LaCl_3 \cdot 7H_2O$	Khimreaktiv	≥99.5
Citric acid $C_6H_8O_7$	Reakhim	≥99
Ethylene glycol $C_2H_6O_2$	Reakhim	≥99
$NH_4H_2PO_4$	Reakhim	≥99
Aqueous NH_3	Khimreaktiv	25, specialty grade
Aqueous HCl	Khimreaktiv	35–38, chemically pure grade
Aqueous HNO_3	Reakhim	65, chemically pure grade
$TiCl_3$	Vecos	15, pure for analysis grade

aqueous NH_3, HCl, and HNO_3, citric acid $C_6H_8O_7$, and ethylene glycol $C_2H_6O_2$. The titanium oxychloride $TiOCl_2$ solution used in the synthesis was prepared by oxidizing a 15% aqueous solution of chemically pure grade $TiCl_3$ by a mixture of concentrated HCl and HNO_3 under air, followed by the gravimetric determination of its concentration [29]. Before use in the synthesis, weighed Y_2O_3 samples were dissolved in nitric acid and $LaCl_3 \cdot 7H_2O$ and $NH_4H_2PO_4$ weights were dissolved in distilled water.

During the synthesis, the solutions of metal salts were mixed in stoichiometric ratios, then citric acid was added to them (in the ratio acid : metal ions = 15 : 1 mol/mol) and dissolved while heated to 60°C. Afterwards, to the thus-prepared mixture of metal citrate complexes, slowly added were ethylene glycol (in the ratio 4 : 1 to the metal ions in the solution) and, simultaneously, ammonium dihydrophosphate to provide a homogeneous gel; the gel was then dried stagewise at 90 (for 48 h), 130 (for 48 h), and 350°C (for 24 h). The precipitate was dispersed, annealed at 500, 550, and 600°C for 72 h at each stage and then at 650 (for 48 h) and 700°C (for 48 h). Each annealing stage was preceded by trituration of the powder mixture with ethanol (as a surfactant) to achieve monodispersity and for mechanical activation to accelerate the synthesis of nanocrystalline materials [30]. The phase composition of the samples after annealing was monitored by X-ray powder diffraction (XRD).

X-ray diffraction experiments were carried out on a Shimadzu XRD-6000 diffractometer. The X-ray diffraction powder patterns were recorded using filtered CuK_α radiation (λ = 1.54178 Å) over the 2θ angle range from 10° to 60° at a scan rate of 1 deg/min with 0.02° scan steps. The *hkl* indices of the synthesized phosphates were determined and their unit cell parameters were calculated based on the structural similarity of the studied compounds to those known from the literature, namely, ($NaTi_2(PO_4)_3$ [18] and $La_{0.33}Ti_2(PO_4)_3$ [26]), and by analytical indexing of X-ray diffraction patterns.

The X-ray diffraction pattern of a $Na_{0.5}Y_{0.165}Ti_2(PO_4)_3$ sample for structural studies was recorded in the 2θ angle range from 13° to 110° in 0.02° steps with an exposure time per point of 12 s. The X-ray diffraction patterns were processed and the phosphate structures refined by the Rietveld method [25] in the Rietan-97 software [26]. The peak profiles were fitted to the modified pseudo-Voigt function (Mod-TCH pV).

To assess the thermal expansion and distortion of the structure upon heating, $Na_{0.5}R_{0.165}Ti_2(PO_4)_3$ (R = Y or La; x = 0.5) phosphates were studied by XRD in the temperature range from 25 to 200°C using an Anton Paar TTK 450 attachment. Linear coefficients of thermal expansion were calculated as a relative increment of the unit cell parameter a or c in response to the one-degree rise in temperature (T): $\alpha_a = \frac{1}{a}\frac{da}{dT}$, $\alpha_c = \frac{1}{c}\frac{dc}{dT}$. The average linear coefficients of thermal expansion were estimated as $\alpha_{avg} = (2\alpha_a + \alpha_c)/3$.

The surface morphology of samples was studied using a Jeol JSM-7600F scanning electron microscope with a thermal-field electron gun (Schottky cathode) at magnifications in the range from ×25 to ×1 × 10^6. The microscope was equipped with a microanalysis system, namely, an Oxford X-Max 80 (Premium) energy-dispersive X-ray spectrometer with a semiconductor silicon drift detector. The uncertainty of electron microprobe analysis in the determination of elemental compositions was 0.5–2.5 mol %.

The IR spectra of the compounds synthesized were recorded on a FTIR-8400 spectrophotometer equipped with an ATR attachment at room temperature in the wavenumber range 1400–400 cm^{-1}. The test samples were phosphate and KBr mixtures compacted to semitransparent disks.

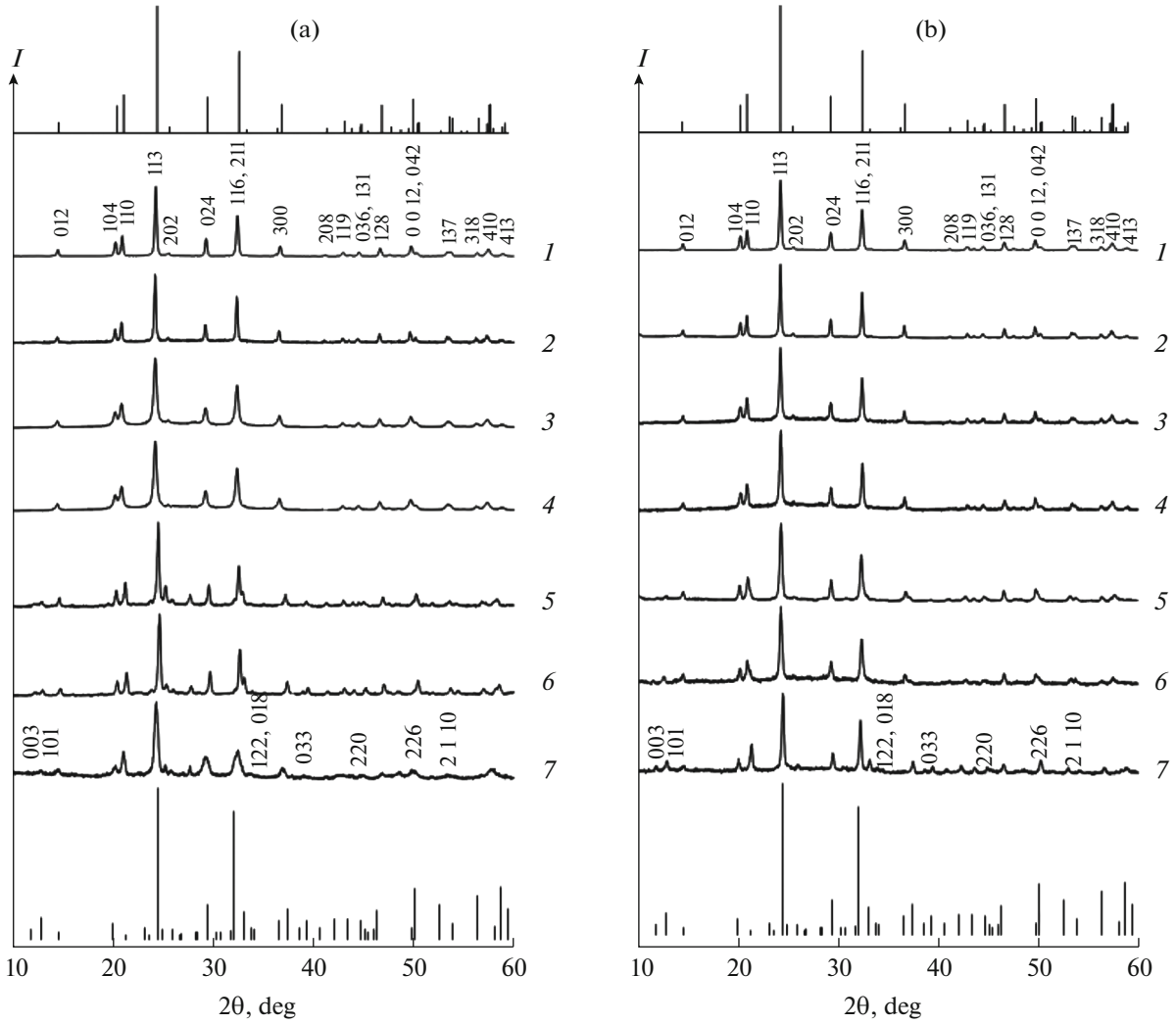

Fig. 1. X-ray diffraction patterns of phosphates: (a) $Na_{1-x}Y_{0.33x}Ti_2(PO_4)_3$, where x = (*1*) 0, (*2*) 0.2, (*3*) 0.5, (*4*) 0.7, (*5*) 0.8, (*6*) 0.9, and (*7*) 1; and (b) $Na_{1-x}La_{0.33x}Ti_2(PO_4)_3$, where x = (*1*) 0, (*2*) 0.2, (*3*) 0.3, (*4*) 0.4, (*5*) 0.5, (*6*) 0.7, and (*7*) 1. The X-ray diffraction bar diagrams refer to $NaTi_2(PO_4)_3$ ($x = 0$) and $La_{0.33}Ti_2(PO_4)_3$ ($x = 1$).

RESULTS AND DISCUSSION

The X-ray diffraction patterns, IR spectra, and electron microprobe analysis imply that the $Na_{1-x}R_{0.33x}Ti_2(PO_4)_3$ (R = Y or La) systems form NZP phosphates. Single-phase phosphates were obtained upon long-term anneals at temperatures from 550 (for $x = 1$) to 700°C (for $x = 0$). Higher annealing temperatures gave rise to the thermal degradation of the NZP phase (above all, in samples with near-unity x values).

Figure 1 shows the X-ray diffraction patterns of the synthesized NZP phosphates. The $0 \le x \le 0.7$ (R = Y) and $0 \le x \le 0.4$ (La) samples were indexed in terms of space group $R\bar{3}c$, the $0.8 \le x \le 1.0$ (Y) and $0.5 \le x \le 1.0$ (La) samples were indexed in terms of space group $R\bar{3}$. The phosphates of space group $R\bar{3}$ featured additional peaks in the X-ray diffraction patterns compared to the phosphate that crystallized in the higher symmetry of space group $R\bar{3}c$.

Electron microscopy and microprobe data verified the homogeneity of the as-synthesized samples and their correspondence to the respective as-batch compositions within the uncertainty of the method.

The IR spectra (Fig. 2) of the synthesized phosphates verify their belonging to orthophosphates with the NZP structure and the absence of X-ray amorphous impurities in the samples.

Factor-group analysis implies that the IR spectra of NZP phosphates with space group $R\bar{3}c$ can feature five bands due to asymmetric stretching vibrations (at 1250–1020 cm^{-1}), one band due to symmetric stretching vibrations (at 1020–950 cm^{-1}), five bands due the asymmetric bending vibrations (at 650–500 cm^{-1}), and two symmetric bending vibrations (at <500 cm^{-1}).

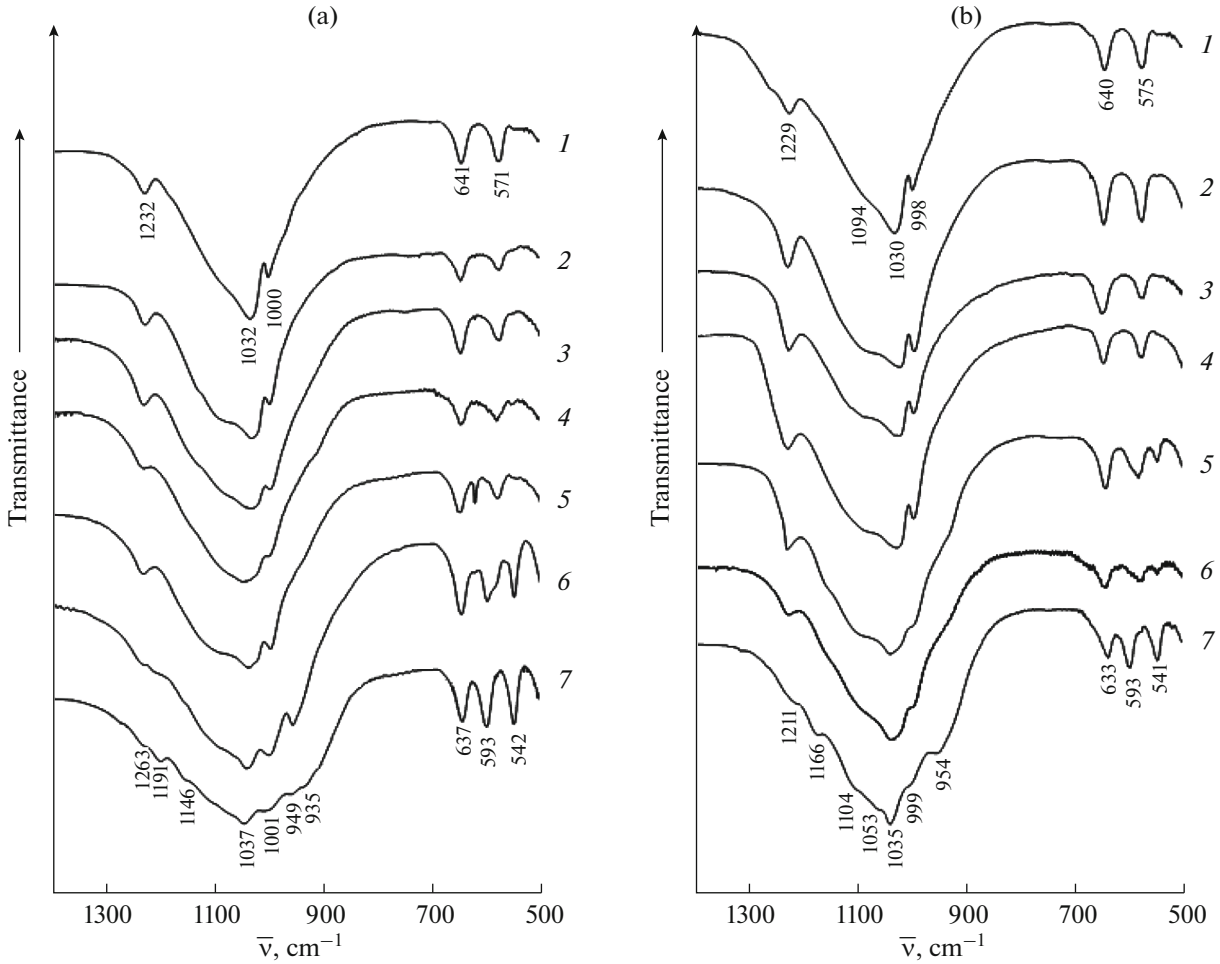

Fig. 2. IR spectra of phosphates: (a) $Na_{1-x}Y_{0.33x}Ti_2(PO_4)_3$, where x = (*1*) 0, (*2*) 0.2, (*3*) 0.5, (*4*) 0.7, (*5*) 0.8, (*6*) 0.9, and (*7*) 1; and (b) $Na_{1-x}La_{0.33x}Ti_2(PO_4)_3$, where x = (*1*) 0, (*2*) 0.2, (*3*) 0.3, (*4*) 0.4, (*5*) 0.5, (*6*) 0.7, and (*7*) 1.

In the IR spectra of the phosphates with space group $R\bar{3}$, selection rules allow to appear six bands of asymmetric stretching vibrations, six bands of asymmetric bending vibrations, two bands of symmetric stretching vibrations, and four bands of symmetric bending vibrations. Thus, the number of the allowed and observed bands of the stretching and bending vibrations was also greater in the spectra of phosphates having a lower symmetry (Fig. 2).

In order to verify the miscibility of sodium and REE in the interstices of the NZP structure in the studied series, we carried out a Rietveld structural study of a $Na_{0.5}Y_{0.165}Ti_2(PO_4)_3$ ($x = 0.5$) sample using X-ray powder diffraction data. An analysis of the X-ray diffraction patterns of this sample according to the absence laws showed that the phosphate crystallized in space group $R\bar{3}c$; therefore, the atomic coordinates in the $NaTi_2(PO_4)_3$ structure served as the initial model [18]. Experimental details and selected refinement results are found in Tables 2–4. Figure 3 shows a good agreement between the measured and calculated X-ray diffraction patterns of the sample.

Figure 4 shows a fragment of the $Na_{0.5}Y_{0.165}Ti_2(PO_4)_3$ crystal structure. The basis of its structure is the $\{[Ti_2(PO_4)_3]^-\}_{3\infty}$ framework, in which the Ti atoms are coordinated by six oxygen atoms of PO_4 tetrahedra. The tetrahedra each share two corners with two octahedra to form a column, and the other two corners use to link to adjacent columns. The octahedrally coordinated positions inside polyhedral columns are shared by Na^+ and Y^{3+} ions, which is evidence of their isomorphic miscibility.

Thus, the results of phase formation studies indicate that isodimorphism is observed in the series of synthesized phosphates $Na_{1-x}R_{0.33x}Ti_2(PO_4)_3$ (R = Y or La), where the terminal solid solutions based on the pure components (x = 0 and 1) crystallize in space groups $R\bar{3}c$ and $R\bar{3}$.

A comparison of phase formation data in the systems studied (Table 5) illustrates a general trend of iso-

Table 2. Details of the experiment, unit cell parameters, and results of crystal structure refinement for $Na_{0.5}Y_{0.165}Ti_2(PO_4)_3$

Space group	$R\bar{3}c$ (№ 167)
Z	6
2θ angle range, deg	13.00–110.00
Unit cell parameters:	
a, Å	8.4983(7)
c, Å	21.8323(15)
V, Å^3	1365.51(18)
Number of reflections	193
Number of refined parameters*	23 + 13
R-factors (%):	
R_{wp}; R_p	3.50; 2.80
S	1.28

* The first figure refers to the background and profile parameters, scale factor, or unit cell parameters; the second figure refers to the positional or thermal parameters of atoms or their site occupancies.

Table 3. Coordinates and isotropic thermal parameters of atoms in the $Na_{0.5}Y_{0.165}Ti_2(PO_4)_3$ structure

Atom	Position	x	y	Z	B, Å^2
Na/Y	6*b*	0	0	0	2.95(2)
Ti	12*c*	0	0	0.14637(9)	0.49(8)
P	18*e*	0.7144(3)	0	0.25	1.53(9)
O(1)	36*f*	0.2011(5)	0.1735(5)	0.3103(2)	1.02(13)
O(2)	36*f*	0.4777(4)	0.3041(5)	0.2482(2)	0.36(11)

Table 4. Selected interatomic distances in the structure-forming polyhedra of $Na_{0.5}Y_{0.165}Ti_2(PO_4)_3$

Bond	d, Å
Na/Y–O(2) (×6)	2.221(4)
Ti–O(1) (×3)	1.863(5)
Ti–O(2) (×3)	2.159(4)
P–O(2) (×2)	1.570(3)
P–O(1) (×2)	1.572(5)

Table 5. Existence areas of NZP solid solutions in the $Na_{1-x}R_{x/3}Ti_2(PO_4)_3$ systems

R	$r(R^{3+})$, Å*	Bounds of x	Space group
Y	0.9	$0 \le x \le 0.7$	$R\bar{3}c$
		$0.8 \le x \le 1.0$	$R\bar{3}$
La	1.03	$0 \le x \le 0.4$	$R\bar{3}c$
		$0.5 \le x \le 1.0$	$R\bar{3}$

* $r(Na^+) = 1.02$ Å.

morphism: an ion of smaller radius enters the crystal structure as an isomorphic impurity more easily than an ion of a larger radius. For the $NaTi_2(PO_4)_3$-base solid solutions (space group $R\bar{3}c$), the variations of chemical composition only insignificantly influence the unit cell parameters (Fig. 5). For the solid solutions where cations are ordered in structural interstices (space group $R\bar{3}$), an even minor change in x gives rise to a considerable increase in unit cell height c and to a

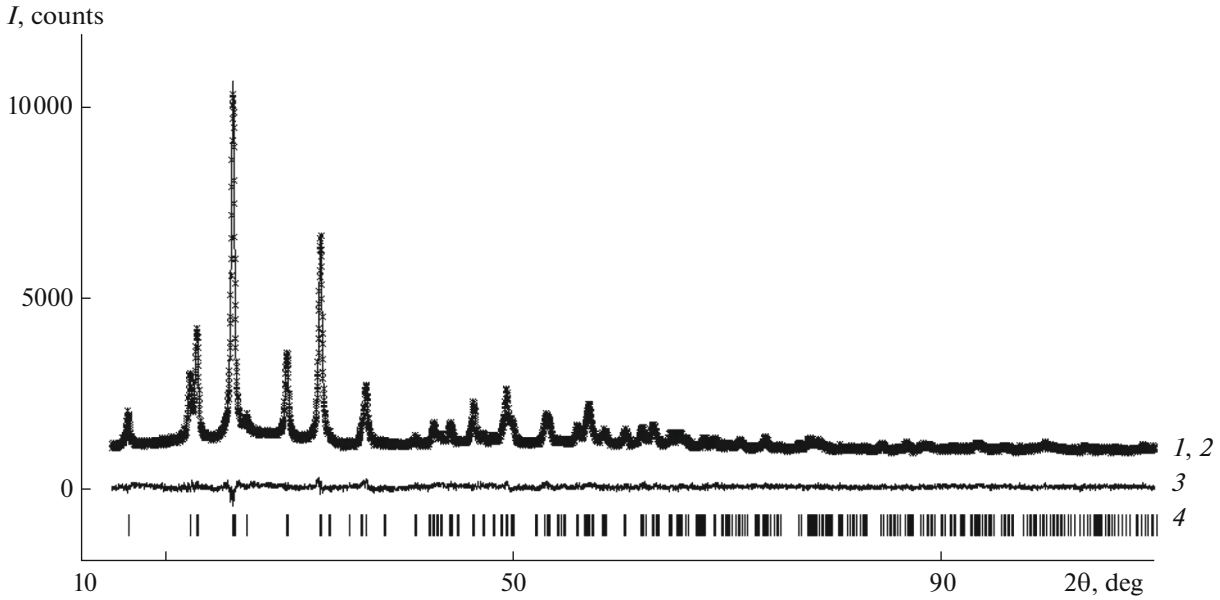

Fig. 3. Fragments of (*1*) measured, (*2*) calculated, and (*3*) difference X-ray diffraction patterns of $Na_{0.5}Y_{0.165}Ti_2(PO_4)_3$; and (*4*) the bar diagram showing Bragg reflection positions.

Table 6. $Na_{0.5}R_{0.165}Ti_2(PO_4)_3$ thermal expansion coefficients in the temperature range from 25 to 200°C

Coefficient	$Na_{0.5}Y_{0.165}Ti_2(PO_4)_3$	$Na_{0.5}La_{0.165}Ti_2(PO_4)_3$
$\alpha_a \times 10^6$, °C^{-1}	–4.5	4.1
$\alpha_c \times 10^6$, °C^{-1}	24.0	20.6
$\lvert\alpha_a - \alpha_c\rvert \times 10^6$, °C^{-1}	28.5	16.6
$\alpha_{avg} \times 10^6$, °C^{-1}	5.0	9.6

decrease in the parameter *a* due to the attendant distortions [1].

The temperature-dependent unit cell parameters of $Na_{0.5}R_{0.165}Ti_2(PO_4)_3$ (R = Y or La; $x = 0.5$) phosphates are plotted in Fig. 6. The increase in interatomic distances in response to rising temperature gives rise to an increase in unit cell height *c* in both samples. The phosphate containing larger interstitial ions (La^{3+}) also has its unit cell parameter *a* increasing as temperature rises. In the case of $Na_{0.5}Y_{0.165}Ti_2(PO_4)_3$ (with smaller interstitial ions), the heating-induced correlated rotation of framework polyhedra induces a decrease in parameter *a*, which is also typical of the NZP compounds [1]. Studies of the thermal expansion of $Na_{0.5}Y_{0.165}Ti_2(PO_4)_3$ and $Na_{0.5}La_{0.165}Ti_2(PO_4)_3$ showed that, because of the negative value of the linear expansion coefficient α_a measured normal to the major third-order axis of a crystal, the value of α_{avg}, the average linear coefficient of thermal expansion, allows the yttrium-containing phosphate to be classified as a material with medium expandability (Table 6). The lanthanum-containing phosphate has a higher α_{avg} value.

CONCLUSIONS

The phase formation of titanium-containing NZP phosphates where rare-earth elements (Y or La) reside in structural cavities has been studied. Isodimorphism has been shown to occur in the series of the synthesized phosphates $Na_{1-x}R_{0.33x}Ti_2(PO_4)_3$ (R = Y or La) to form terminal solid solutions whose structures differ from one another in the extent of cation ordering in interstices. Structural data has verified the results of our study. Thermal expansion studies of $Na_{0.5}Y_{0.165}Ti_2(PO_4)_3$ and $Na_{0.5}La_{0.165}Ti_2(PO_4)_3$ have shown that the distortions of their unit cells upon heating are largely determined by the sizes of cations in the interstices.

CONFLICT OF INTEREST

The authors declare that they have no conflicts of interest.

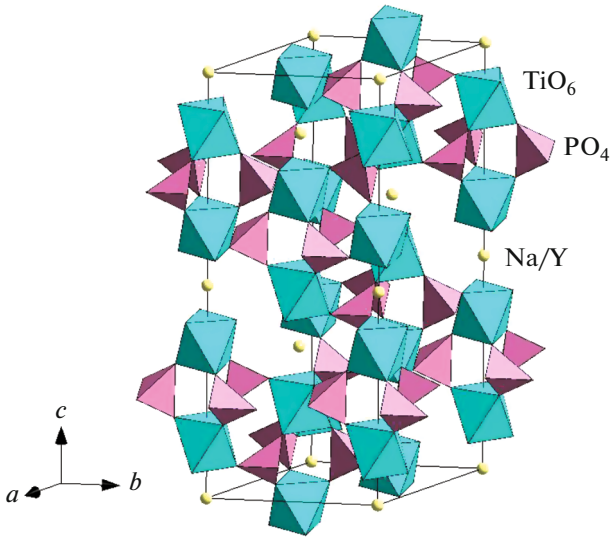

Fig. 4. Fragment of the $Na_{0.5}Y_{0.165}Ti_2(PO_4)_3$ crystal structure.

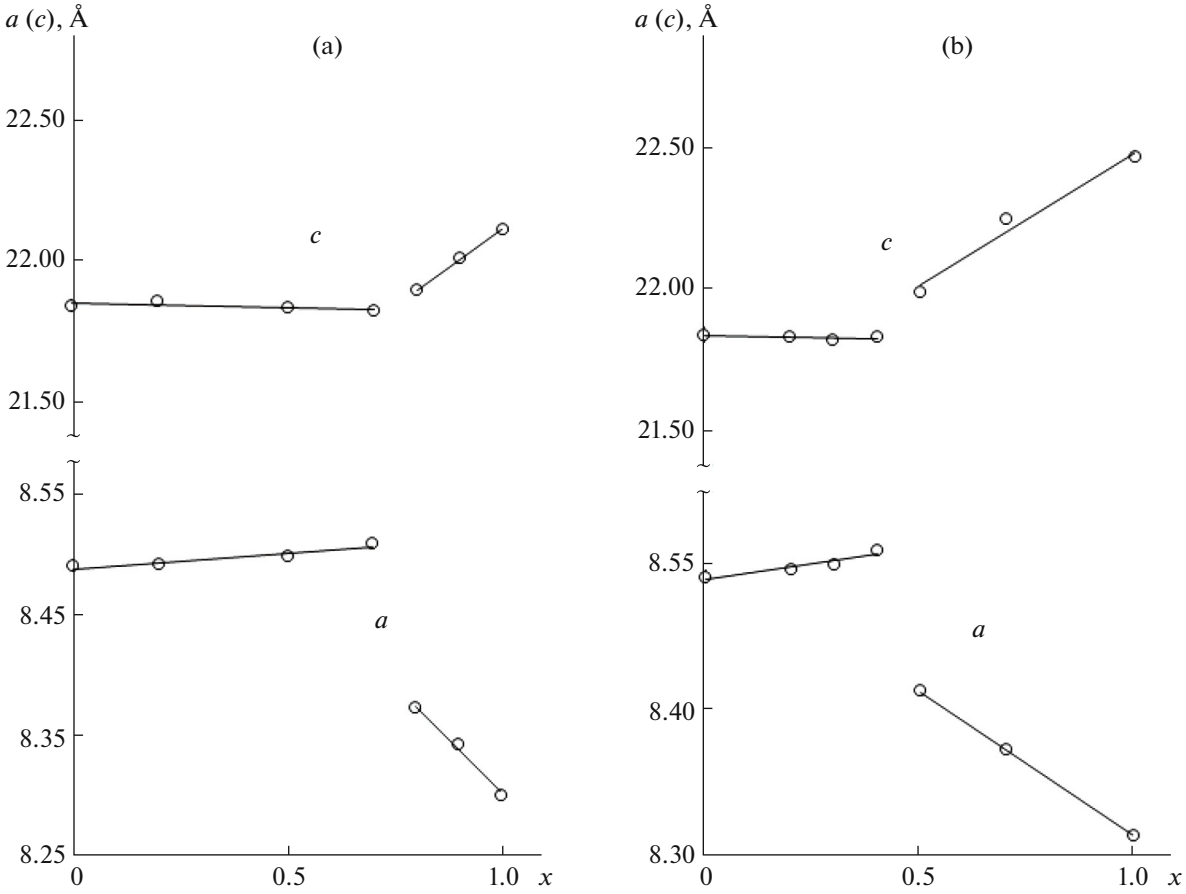

Fig. 5. Unit cell parameters of phosphates versus chemical composition (x) for (a) $Na_{1-x}Y_{0.33x}Ti_2(PO_4)_3$ and (b) $Na_{1-x}La_{0.33x}Ti_2(PO_4)_3$.

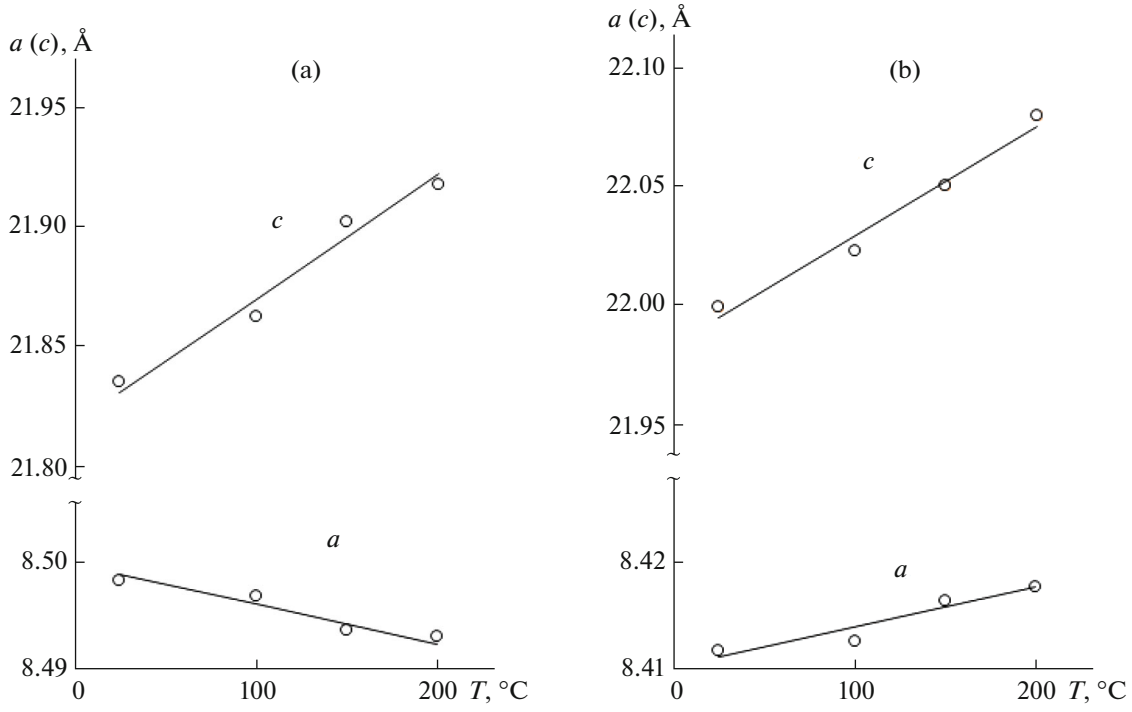

Fig. 6. Unit cell parameters versus temperature for (a) $Na_{0.5}Y_{0.165}Ti_2(PO_4)_3$ and (b) $Na_{0.5}La_{0.165}Ti_2(PO_4)_3$.

REFERENCES

1. V. I. Pet'kov and E. A. Asabina, Glass Ceram. **61**, 233 (2004). https://doi.org/10.1023/B:GLAC.0000048353.42467.0a
2. M. I. Kimpa, M. Z. H. Mayzan, J. A. Yabagi, et al., IOP Conf. Series: Earth Environ. Sci. **140**, 012156 (2018). https://doi.org/10.1088/1755-1315/140/1/012156
3. S. Naqash, M. -Th. Gerhards, F. Tietz, et al., Batteries **4**, 33 (2018). https://doi.org/10.3390/batteries4030033
4. N. Anantharamulu, K. Koteswara Rao, G. Rambabu, et al., J. Mater. Sci. **46**, 2821 (2011). https://doi.org/10.1007/s10853-011-5302-5
5. G. B. Kunshina and I. V. Bocharova, Glass. Phys. Chem. **46**, 576 (2020). https://doi.org/10.1134/S1087659620060140
6. E. A. Kurzina, I. A. Stenina, A. Dalvi, et al., Inorg. Mater. **57**, 1035 (2021). https://doi.org/10.1134/S0020168521100071
7. S. N. Achary, S. Bevara, and A. K. Tyagi, Coord. Chem. Rev. **340**, 266 (2017). https://doi.org/10.1016/j.ccr.2017.03.006
8. N. I. Steblevskaya, M. V. Belobeletskaya, A. Yu. Ustinov, et al., Russ. J. Inorg. Chem. **64**, 179 (2019). https://doi.org/10.1134/S0036023619020219
9. C. A. Kodaira, H. F. Brito, O. L. Malta, et al., J. Lumin. **101**, 11 (2003).
10. M. Lin, Y. Zhao, S. Wang, et al., Biotechnol. Adv. **30**, 1551 (2012).
11. X. He, J. Huang, L. Zhou, and et al., Cent. Eur. J. Phys. **10**, 514 (2012). https://doi.org/10.2478/s11534-012-0014-2
12. A. E. Kanunov and A. I. Orlova, Rev. J. Chem. **8**, 1 (2018). https://doi.org/10.1134/S207997801801003X
13. B. Glorieux, V. Jubera, A. I. Orlova, et al., Inorg. Mater. **49**, 82 (2013). https://doi.org/10.1134/S0020168513010032
14. M. Hirayama, N. Sonoyama, A. Yamada, et al., J. Solid State Chem. **182**, 730 (2009). https://doi.org/10.1016/j.jssc.2008.12.015
15. J. Wang and Z.-J. Zhang, J. Alloys Compd. **685**, 841 (2016). https://doi.org/10.1016/j.jallcom.2016.06.224
16. A. E. Shvetsov and A. K. Koryttseva, Russ. J. Gen. Chem. **85**, 359 (2015). https://doi.org/10.1134/S1070363215030020
17. N. S. Slobodyanik, P. G. Nagornyi, Z. I. Kornienko, et al., Zh. Neorg. Khim. **33**, 443 (1988).
18. I. V. Zatovsky, N. S. Slobodyanik, D. A. Stratiychuk, et al., Z. Naturforsch., B: Chem. Sci. **55**, 291 (2000). https://doi.org/10.1515/znb-2000-3-411
19. D. M. Bykov, E. R. Gobechiya, Yu. K. Kabalov, et al., J. Solid State Chem. **179**, 3101 (2006). https://doi.org/10.1016/j.jssc.2006.06.002
20. M. Barre, *These Presentee a L'Universite du Maine pour Obtenir le Titre de Docteur de L'Universite du Maine*, Mention Chimie de l'Etat Solide, 2007.
21. M. Barre and M. P. Crosnier-Lopez, F. Le Berre, et al., Chem. Mater. **17**, 6605 (2005).
22. M. Barre, F. Le Berre, M. P. Crosnier-Lopez, et al., Chem. Mater. **18**, 5486 (2006).
23. V. S. Kurazhkovskaya, D. M. Bykov, E. Yu. Borovikova, et al., Vibrat. Spectrosc. **52**, 137 (2010).
24. A. Kanunov, A. Orlova, G. Zavedeeva, et al., Bull. Mater. Sci. **40**, 7 (2017). https://doi.org/10.1007/s12034-016-1337-1
25. P. Lightfoot, D. A. Woodcock, J. D. Jorgensen, et al., Int. J. Inorg. Mater. **1**, 53 (1999).
26. E. A. Asabina, R. R. Shvarev, V. I. Pet'kov, et at., Russ. J. Inorg. Chem. **62**, 1215 (2017). https://doi.org/10.1134/S0036023617090029
27. R. D. Shannon, Acta Crystallogr., Sect. A **32**, 751 (1976).
28. A. Matraszek, P. Godlewska, L. Macalik, et al., Alloys Compd. **619**, 275 (2015).
29. E. László, *International Series of Monographs on Analytical Chemistry, Gravimetric Analysis* (Pergamon: Elsevier, 1965).
30. A. M. Kalinkin, O. A. Kuz'menkov, E. V. Kalinkina, et al., Russ. J. Gen. Chem. **92**, 1056 (2022). https://doi.org/10.1134/S1070363222060172

Translated by O. Fedorova